Geophysical Research Letters

RESEARCH LETTER
10.1029/2022GL098885

Key Points:

- A 1D deltaic island model produces secondary channels that undergo autogenic discharge oscillations
- Secondary channels provide a mechanism for maintaining island sedimentation that keeps pace with sea level
- Secondary channels can grow to become stable primary channels, limiting the maximum island size

Supporting Information:

Supporting Information may be found in the online version of this article.

Correspondence to:

G. Salter,
gsalter@usgs.gov

Citation:

Salter, G., & Lamb, M. P. (2022). Autocyclic secondary channels stabilize deltaic islands undergoing relative sea level rise. *Geophysical Research Letters*, *49*, e2022GL098885. https://doi.org/10.1029/2022GL098885

Received 26 MAR 2022
Accepted 14 JUL 2022

Autocyclic Secondary Channels Stabilize Deltaic Islands Undergoing Relative Sea Level Rise

Gerard Salter[1,2] and Michael P. Lamb[1]

[1]Division of Geological and Planetary Sciences, California Institute of Technology, Pasadena, CA, USA, [2]Now at U.S. Geological Survey, Southwest Biological Science Center, Grand Canyon Monitoring and Research Center, Flagstaff, AZ, USA

Abstract Understanding what sets the size and stability of deltaic islands is critical for predicting how deltas will respond to sea level rise. Models of overbank sedimentation produce an exponentially decaying sedimentation profile, seemingly incompatible with island stability, which requires uniform sedimentation balancing sea level rise. However, secondary channels provide a mechanism for delivering sediment deeper into island interiors, potentially stabilizing islands. Using a 1D morphodynamic model, we found that autogenic secondary channels allow islands or parts of islands to maintain a stable profile dynamically through cycles of channel incision and aggradation. However, when islands are too large, secondary channels grow to become stable, primary channels, thereby bisecting the island, resulting in smaller, stable islands with more connectivity to the channel network. Rather than passively drowning, our results indicate that deltaic islands can respond to sea level rise through morphodynamic feedbacks that act to enhance island accretion.

Plain Language Summary River deltas are low-lying coastal landscapes, making them vulnerable to sea level rise. Deltas are commonly composed of islands separated by river channels. These islands are formed and maintained by sediment supply delivered from the surrounding river channels. Here, we develop a numerical model to explain how sediment is delivered to islands, and how this sediment allows islands to build land vertically, potentially allowing them to keep pace with rising sea level rather than passively drowning. We find that small channels can deliver sediment from river channels to island interiors, allowing islands to keep pace with sea level. Our model predicts that these small channels undergo natural cycles of deepening and shallowing, consistent with observations. Additionally, our model predicts that large islands are eventually split by larger permanent river channels, whereas small islands tend to merge, potentially explaining the range of island sizes found in river deltas. Overall, our model shows that deltaic islands undergoing sea level rise do not passively drown, but rather activate secondary channels and change their size to allow vertical land building to keep pace with sea level.

1. Introduction

Deltas worldwide are home to over 300 million people (Edmonds et al., 2020), and are threatened with widespread land loss due to their naturally low elevation, increasing relative sea level rise (RSLR), and reduced sediment supply (Hoitink et al., 2020; Nienhuis et al., 2020). Deltaic islands represent the primary land-building unit of active delta topsets, buffer storm surge, and store carbon (Paola et al., 2011; Shields et al., 2017). Therefore, understanding what sets the size and shape of deltaic islands and how they respond to RSLR is critical for assessing the vulnerability of deltas, developing sustainable delta management strategies, and climate adaptation.

Deltaic islands are bound by relatively persistent channel networks (Figure 1). Island size, as measured via the island half-width, is typically on the order of hundreds of channel depths (Figure 1). Smaller secondary channels connect the primary channels to island interiors, and can grow and anneal on decadal time scales (Figure 1). The mechanisms producing secondary channels and their role in nourishing island interiors to combat RSLR remain poorly constrained (Esposito et al., 2020; Hiatt & Passalacqua, 2015).

An island may be considered stable if its aggradation rate balances RSLR. The aggradation rate is sometimes approximated as uniform (Giosan et al., 2014), however, advection and settling models predict sedimentation rates that decline exponentially toward island interiors (Day et al., 2008). In that case, islands might be unstable and respond to RSLR through drowning of their interiors. However, secondary channels provide a potential

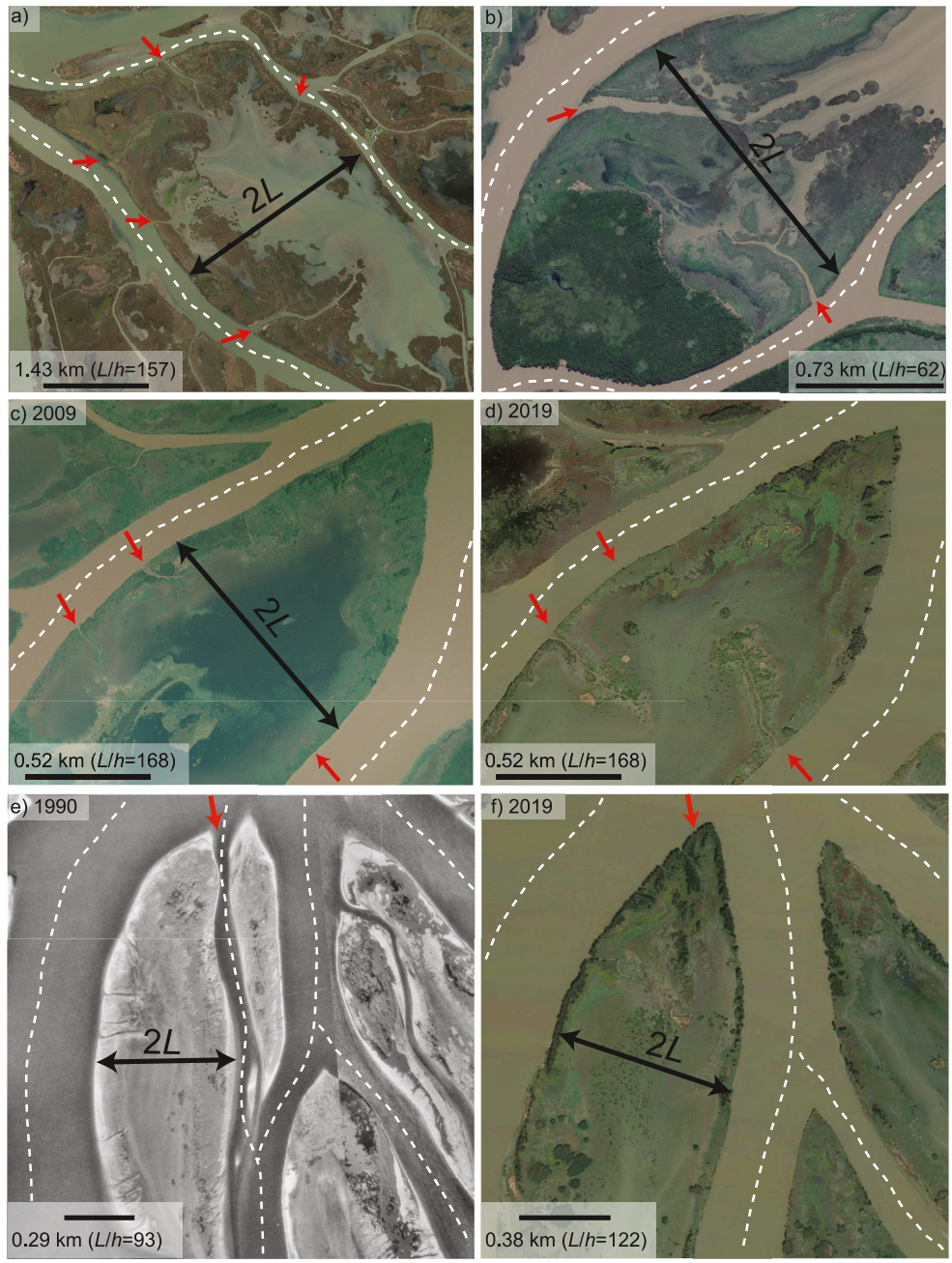

Figure 1. Satellite imagery of deltaic islands from Google Earth, with red arrows indicating secondary channels, and white dashed lines tracing primary channels. Scale bars indicate approximate island size *L*, characterized by the half-width, where *h* is the primary channel depth. (a) Mississippi River Delta, Louisiana, USA. (b) Paraná River Delta. (c–f) Wax Lake Delta, Louisiana, USA in 2009, 2019, 1990, and 2019 respectively. Pairs (c and d) and (e and f) are at the same location.

mechanism to nourish island interiors (Nienhuis et al., 2018; Rowland et al., 2009; Slingerland & Smith, 1998), potentially accounting for the sediment deficit left from overbank advection-settling.

We hypothesize that—whereas overbank sedimentation, modeled via advection and settling, results in an exponential sedimentation profile, because there is no mechanism for removing sediment once it is deposited—the addition of bed sediment entrainment in conjunction with advection/settling is sufficient to generate autogenic secondary channels. Here, rather than treating islands as landforms with a fixed geometry, we built a morphodynamic model to explore how these two mechanisms control deltaic island size and response to RSLR. Even

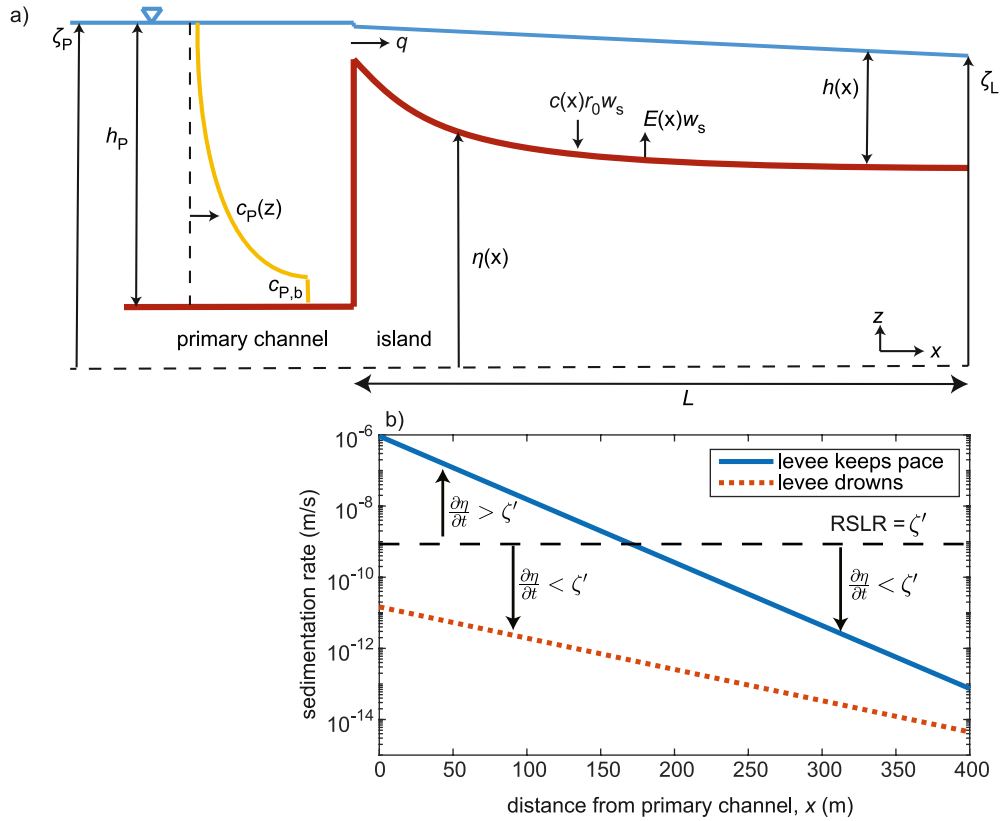

Figure 2. (a) Schematic of our model showing the primary channel boundary condition, and the bed elevation $\eta(x)$ of the island from $x = 0$ to $x = L$. h_P, c_P, and ζ_P are the primary channel depth, concentration, and water level, respectively. q is the unit water discharge, $c(x)$ and $E(x)$ are the concentration and entrainment, respectively, $h(x)$ is the water depth, w_s is the settling velocity, r_0 is the mean to near-bed concentration ratio, and ζ_L is the downstream water level. (b) Example of sedimentation rate profiles where levee sedimentation keeps pace with relative sea level rise, and an example where the entire island drowns.

though our model is highly simplified, it generates complex and unanticipated behavior. Using a simplified model allows us to probe parameter space and better understand a new potential mechanism by which islands accrete in response to RSLR.

2. Methods

We developed a 1D model of a deltaic island representing a transect with an evolving bed from the island edge to its interior (Figure 2). To find whether secondary channels alone can produce stable islands, we neglected other potentially important island processes: vegetation, which affects roughness (Baptist et al., 2007), and produces aggradation via organic accretion (Kirwan et al., 2010; Lorenzo-Trueba et al., 2012), 2D effects such as flow spreading and interactions between secondary channels, stratification effects on the primary channel vertical concentration profile, and we assumed a single bed-material grain size.

Water depth, h, was calculated from the gradually varied flow equation:

$$\frac{dh}{dx} = \frac{-\frac{d\eta}{dx} - c_f Fr^2}{1 - Fr^2} \tag{1}$$

where η is bed elevation, x is distance from primary channel, c_f is friction coefficient, and Fr is Froude number (Text S1 in Supporting Information S1; Chow, 1959). We set $c_f = 0.01$ based on small sand-bed rivers (Trampush et al., 2014). The downstream boundary was specified by sea level ζ_L, increasing at a constant rate of RSLR.

In order to find the unit discharge entering the island q, Equation 1 was iterated such that the water level at the upstream boundary matched the primary channel water level ζ_P, written:

$$\zeta_P = \eta(0) + h(0) + \frac{q^2}{2gh(0)^2} \tag{2}$$

where the final term represents a correction for the conversion of potential energy to kinetic energy (Sturm, 2010). We assumed a constant water surface slope $\frac{\zeta_P - \zeta_L}{L}$ across the island, implying that the primary channel water level rises at the same rate as the sea level at the downstream boundary. For simulations modeled after specific deltas, we assumed an island water surface slope of twice the delta down-channel water surface slope unless otherwise specified, consistent with observations (Hiatt & Passalacqua, 2017); model sensitivity to this choice is explored in Section 5.

We solved for depth-averaged sediment concentration over the island, $c(x)$, by mass balance (Parker, 2004):

$$\frac{dc}{dx} = (-r_0 c + E)\frac{w_s}{q} \tag{3}$$

where r_0 is the ratio of depth-averaged to near-bed sediment concentration (Parker et al., 1987), w_s is the settling velocity, and E is entrainment of bed sediment, calculated according to van Rijn (1984) and Brownlie (1981) (Text S1 in Supporting Information S1). For simplicity, we used $r_0 = 7$ (Text S1 in Supporting Information S1) and explored sensitivity to this choice (Figure S1 in Supporting Information S1). We found $c(0)$ by averaging the Rouse profile from the primary channel (Rouse, 1937; Vanoni, 1946) over the depth of the flow entering the island ($z = \zeta_P - h(0)$ to $z = \zeta_P$; Text S1 in Supporting Information S1). The bed evolved through time according to mass conservation:

$$\frac{\partial \eta}{\partial t} = \frac{(r_0 c - E)\, w_s}{1 - \lambda} \tag{4}$$

where λ is the bed porosity.

3. Zero-Entrainment Model

When sediment entrainment is $E = 0$, Equation 3 can be integrated and substituted into Equation 4 to yield an exponential sedimentation profile:

$$\frac{\partial \eta}{\partial t} = \frac{c(0) r_0 w_s}{1 - \lambda} e^{\frac{-r_0 w_s x}{q}} \tag{5}$$

The quantity $\frac{q}{w_s r_0}$ is known as the advection length (Ganti et al., 2014), which is the characteristic distance traveled by an advected sediment particle before settling to the bed. A small advection length implies a rapid decay in sedimentation, with sedimentation focused near the island edge, whereas a large advection length yields closer to uniform sedimentation into the island interior. Depending on the balance between sedimentation and RSLR, part or all of the island may drown (Figure 2b).

Results show that when sedimentation rate at the upstream island edge exceeds RSLR, in which case the depth over the levee decreases, the concentration $c(0)$ set by the primary channel Rouse profile decreases accordingly. Eventually, due to the decreased sediment concentration, the levee sedimentation rate matches RSLR. Under this condition, the island interior gradually drowns due to slow sedimentation associated with the exponential sedimentation rate profile, while the levee keeps pace (Figure S2 in Supporting Information S1, Movie S1). A second possibility is that even the maximum $c(0)$ is insufficient for sedimentation to keep pace with RSLR, in which case the entire island drowns (Figure S3 in Supporting Information S1, Movie S2).

Although a large advection length allows for increased sediment delivery to the island interior, potentially resulting in a stable island profile, it also results in reduced sediment retention, with sediment bypassing the island altogether. This tradeoff is illustrated by integrating $\frac{\partial \eta}{\partial t}$ over the domain length L:

$$\int_0^L \frac{\partial \eta}{\partial t}\, dx = \frac{q c(0)}{1 - \lambda}\left(1 - e^{\frac{-r_0 w_s L}{q}}\right) \tag{6}$$

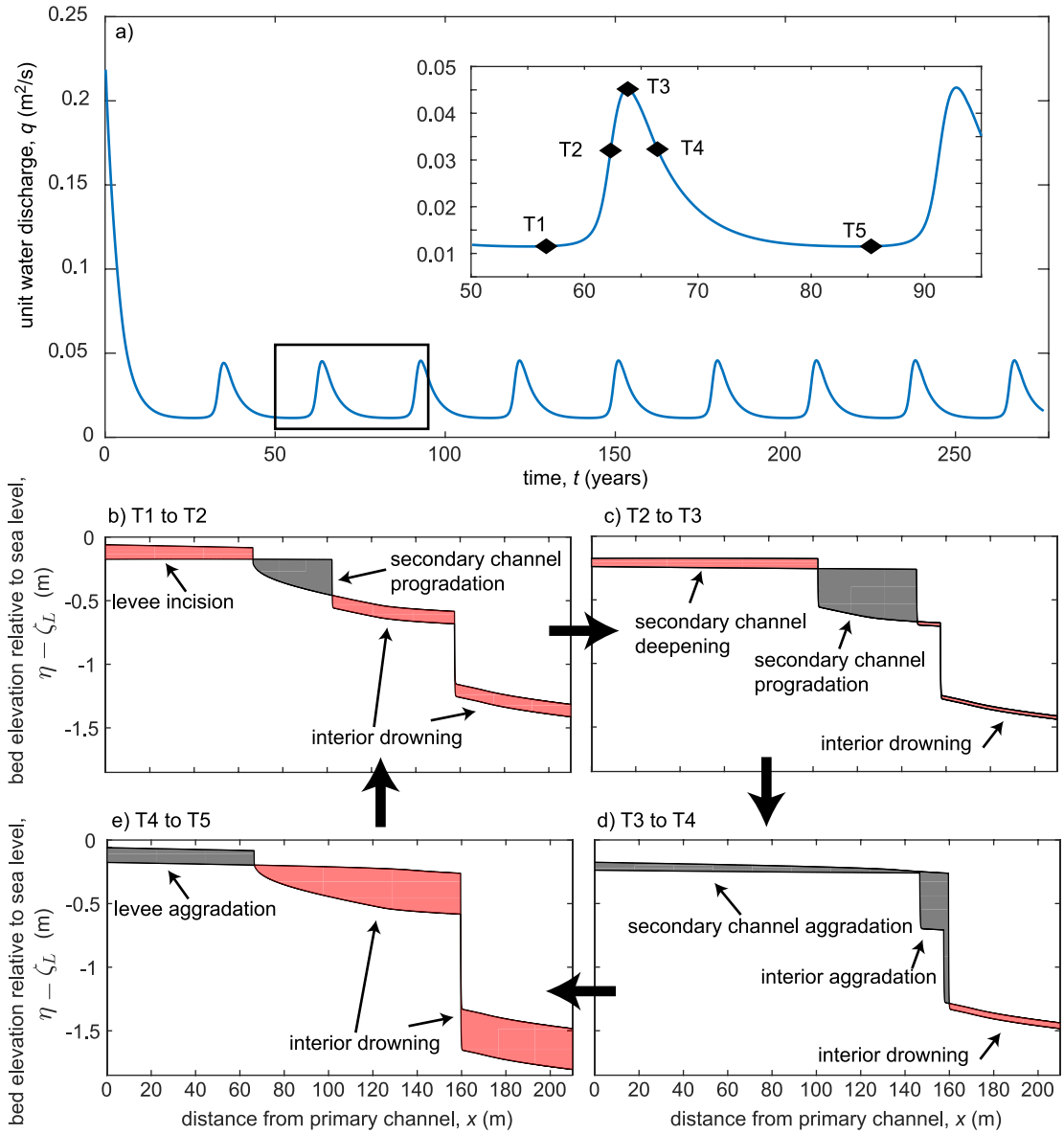

Figure 3. (a) Example time series of unit water discharge q for the oscillating regime. (b–e) Oscillating regime bed elevation profiles referenced to sea level ($\eta(x) - \zeta_L$) at times indicated in the panel (a) inset. Red shaded regions indicate a decrease in bed elevation relative to sea level due to drowning and/or erosion; gray shaded regions indicate an increase in relative bed elevation.

From Equation 6, as the ratio of advection length to island size L increases, a decreasing fraction of the incoming sediment supply is retained within the island (Figure S4 in Supporting Information S1). Thus, while large advection lengths may be one possible way to sustain uniform deposition, a small fraction of sediment is retained on the island, and therefore, this is unlikely to be sufficient for islands to maintain stability under high RSLR.

4. Stable and Unstable Island Regimes

We considered model behavior with bed sediment entrainment included. We found two regimes of island dynamics. The first is an oscillating regime (Figure 3a, Movie S3), where the island maintained a stable profile on average but the discharge into the island fluctuated autogenically, which we interpreted as secondary channel growth through incision followed by aggradation and annealing. Instantaneous sedimentation rates did not match RSLR. However, averaged over a cycle of secondary channel incision and aggradation, sedimentation matched RSLR.

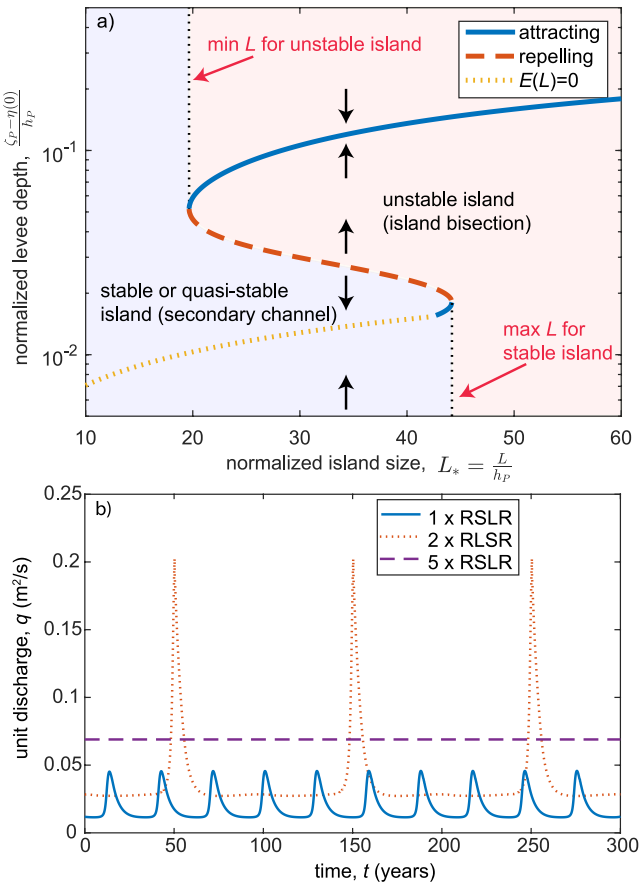

Figure 4. (a) Island stability phase space as a function of normalized island size L_* and normalized levee depth $\frac{\zeta_P-\eta(0)}{h_P}$, where $L_* = \frac{L}{h_P}$, L is the island size, and ζ_P and h_P are the primary channel water level and depth, respectively. Red shaded region represents an unstable island, and blue shaded region represents a stable island. Black arrows indicate increasing or decreasing depth through time for a given initial condition. Curves represent attracting and repelling steady state solutions, and levee depth corresponding to zero entrainment at island end, that is, $E(L) = 0$. (b) Oscillating regime unit water discharge time series $q(t)$; curves correspond to differing relative sea level rise.

We explored the physical mechanisms driving oscillations through an example modeled after the Mississippi River Delta (Figure 3). At time T1, sedimentation in the upstream part of the island balanced sea level, but the interior drowned due to the exponential falloff in sedimentation expected from advection and settling (Figure 3b). Drowning resulted in increased interior depth, yielding a shallower water surface slope across the interior (increased water depth conveys the same water discharge at a decreased slope), and therefore a steepened surface slope over the levee to match the primary channel water level. The steepened upstream slope increased q, causing entrainment, E, to increase and exceed the settling flux relative to RSLR. Therefore, from T1-T2, the flow depth began to increase, triggering a positive feedback where increased upstream flow depth increased q, which in turn increased E. As the upstream part of the secondary channel continued to incise, it conveyed sediment toward the island interior, causing island interior aggradation via secondary channel progradation (Figure 3b). From T2-T3, upstream incision and progradation continued, producing relief between the new deposit and the antecedent drowned topography (Figure 3c). Eventually, at T3, q began to decrease due to (a) increased $c(0)$ by tapping into the deeper, higher concentration portion of the primary channel concentration-depth profile, increasing levee sedimentation, and (b) decreased interior flow depth due to aggradation, which caused the levee water surface slope to decrease (similar to the slope increase caused by interior drowning explained above). As q declined, the upstream portion of the island aggraded because of reduced E, while the island interior resumed drowning due to reduced sediment supply (Figure 3d). At T4, the secondary channel continued to aggrade, cutting off sediment supply to the island interior, causing further drowning (Figure 3e), setting up the condition for the cycle to repeat (T1).

Through the mechanism of secondary channel growth and annealing, the majority of the island achieved a quasi-steady regime where it aggraded at a pace equal to RSLR when averaged over many secondary channel growth cycles. However, in this example, the far downstream part of the island drowned continuously, analogous to the quasi-stable condition observed for the zero-entrainment model, because the island water surface slope was insufficient to drive sediment to the downstream island edge. The oscillating regime represents a stable or quasi-stable island condition, depending on whether the entirety of the island keeps pace with RSLR. For the Mississippi scenario, along with other deltas with parameter values obtained from Chadwick et al. (2020), we obtained oscillation periods on the order of tens to hundreds of years (Figures 3a and 4b, Table S1 in Supporting Information S1), consistent with growth and annealing over decades in Figures 1c–1f.

In addition to the oscillating regime, which forms quasi-steady island topography, the model produced an additional regime where the secondary channel grew to become a stable, primary channel (Movie S4). In this regime, the instantaneous sedimentation rate balanced RSLR across the entire island length, that is, $\frac{\partial \eta}{\partial t}(x) = \zeta_L'$. Substituting this condition into Equations 3 and 4 yields:

$$c(x) = c(0) - \frac{\zeta_L'(1-\lambda)}{q}x \tag{7}$$

$$E(x) = r_0 c(x) - \frac{\zeta_L'(1-\lambda)}{w_s} \tag{8}$$

which represents a steady state, where both concentration and entrainment decrease linearly across the island. The steady state channel is relatively deep, and there is a balance between sediment settling and entrainment and RSLR, similar to any alluvial river channel at topographic steady state. Therefore, we interpret the steady state

condition as a primary channel. This regime therefore corresponds to an unstable island size, that is, the channel would be a stable feature splitting the island into two islands, not a secondary channel nourishing the island interior.

To explore whether islands tend toward bisection or remain within the oscillating regime, we developed a procedure for solving for the steady state island profile $\eta(x)$ and corresponding levee depth $h(0)$, and determining whether the solution is attracting or repelling (Text S2 and Figure S5 in Supporting Information S1). Additionally, we found the minimum discharge for sediment supply to maintain the island ($E(L) = 0$). We defined a phase space for island stability in terms of normalized levee depth $\frac{\zeta_P - \eta(0)}{h_P}$ and normalized island size $L_* = L/h_P$ (Figure 4a, Figure S6 in Supporting Information S1). For a given L_*, and an initial depth greater than the repelling steady state, the island will tend toward the attracting steady state solution, representing island bisection. Alternatively, for an initial depth less than the repelling steady state, the depth decreases initially, and islands tend toward the oscillating regime, representing a stable or quasi-stable island. The attracting and repelling steady state solutions intersect in a saddle-node bifurcation. For L_* smaller than this intersection point, islands are inevitably stable, because entrainment is insufficient to maintain a steady state solution, resulting in the oscillating regime. Additionally, for large island sizes, there is no repelling steady state, and the island is inevitably bisected, because a secondary channel would not provide adequate sediment supply for the island to keep pace with RSLR. For intermediate island sizes, both stable and unstable islands are possible, depending on the initial condition. Complicating this picture, for some simulations within the oscillating regime, we found that the water discharge overshoots during the secondary channel growth stage, causing the island to tend toward the unstable regime (Figure S7 in Supporting Information S1).

Island size primarily influences stability through its effect on the water level gradient of the island. Although the water level difference between ζ_P to ζ_L is linearly proportional to L_*, the water level drop due to the energy correction in Equation 8 is independent of L; therefore, the water level gradient increases with L_*. For low L_*, the water level gradient is insufficient to drive sufficient entrainment to satisfy (Equation 8), so no steady state solutions are obtained (Figure 4a). For larger L_*, two steady state solutions are obtained, one at low depth and one at high depth. The low-depth solution is repelling, because an increase in depth triggers a larger increase in entrainment (via increased discharge) than it does input sediment concentration (depth increase leads to runaway erosion; depth decrease leads to runaway sedimentation). The high-depth solution is attracting, because increased depth causes input sediment concentration to increase more rapidly than entrainment. Finally, for the $E(L) = 0$ curve, depth increases with L_* in order for the channel to convey increased q, because larger islands require higher sediment input to keep pace with sea level; the approach of this curve toward the repelling steady state limits maximum island size.

5. Model Sensitivity Analysis

We explored the effect of RSLR on the stable island (oscillating) regime. Figure 4b shows $q(t)$ for different RSLR, holding all other parameters constant, based on the Mississippi River Delta. As RSLR increases, the minimum and mean q entering the island increase, implying that increased RSLR results in larger, more persistent secondary channels. This response allows secondary channels to deliver and deposit more sediment in order to compensate for the increased rate of accommodation generation due to RSLR. The response of oscillation amplitude and period is more complex: a doubling of RSLR caused less frequent but larger oscillations, but increasing RSLR by a factor of five resulted in a steady state solution, because the increased RSLR kept interior depths high, preventing secondary channel annealing. The range of stable island sizes is also affected by RSLR (Figure 5a), particularly the maximum stable island size. This is because for a fixed sediment supply, larger RSLR requires a smaller island size for sediment supply to exactly balance accommodation generation. Additionally, secondary channels may nourish an area wider than their width. To test the effect of nourishment width, that is, the width maintained by sedimentation from a single secondary channel, we scaled bed elevation change through Equation 4 by the ratio of secondary channel width to nourishment width, and we found increased nourishment width decreases oscillation period (Figure S8 in Supporting Information S1).

Island size predictions are sensitive to island water surface slope (Figure 5b). We assumed for our Mississippi scenario that the island water slope was twice the delta slope. The minimum unstable island size increases dramatically as slope decreases, because larger island sizes produce a larger internal water level gradient within

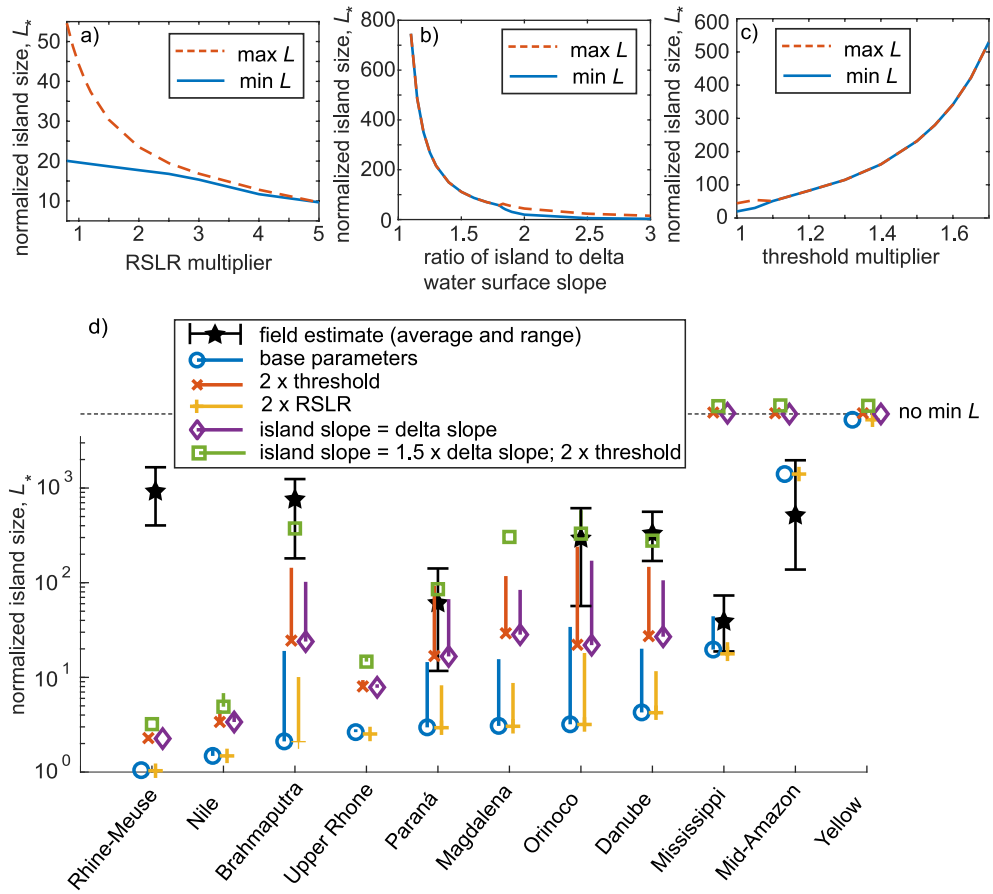

Figure 5. (a–d) Minimum normalized island size L_* for bisection, and maximum L_* for stability, where $L_* = \frac{L}{h_p}$, L is the island size, and h_p is the primary channel depth, for conditions modeled after the Mississippi River Delta. L_* values are plotted against (a) factor multiplying the relative sea level rise (RSLR) rate, (b) delta to island water surface slope ratio, and (c) factor multiplying the bed sediment entrainment threshold. (d) Sensitivity of L_* range to RSLR, entrainment threshold, and island slope using field delta parameters from Chadwick et al. (2020). Lines span the minimum island size for bisection to the maximum size for stability. For comparison, the average and range of island sizes within the active delta topset of the deltas was estimated from satellite images (Figures S12–S18 in Supporting Information S1).

the island. As L_* increases, the internal water level gradient approaches the imposed slope. For low island slopes, entrainment is insufficient to satisfy (Equation 8), so no minimum island size is obtained. Additionally, in Figure 5b, for island-to-delta slope ratios less than around 1.8, the maximum and minimum island sizes are relatively large. Here, the maximum and minimum island sizes coincide because larger islands require a larger q to drive sufficient sediment supply to balance accommodation generation, causing the repelling steady state to disappear.

Next, we investigated model sensitivity to the entrainment threshold τ_{*cr}, which can be influenced by cohesive sediment or vegetation. Increasing τ_{*cr} caused a shift toward larger island sizes (Figure 5c and Figure S9 in Supporting Information S1); in Figure 5c, a less than factor-of-two increase triggered an island size increase by two orders of magnitude. This occurs because increased entrainment threshold necessitates a higher water level gradient for the steady state entrainment profile (Equation 8), and to increase the effective island water level gradient, L_* must increase.

Figure 5d shows the predicted range of island sizes for various deltas with parameter values obtained from Chadwick et al. (2020), from the minimum size for bisection to the maximum size for stability (Text S1 and Figure S10 in Supporting Information S1). Our intention is not to compare the island size distributions between deltas in detail, but rather to show that model sensitivity trends are consistent across a range of realistic base

parameters. We found that an increase in entrainment threshold or decrease in slope increases stable island sizes, and an increase in RSLR decreases the maximum stable island size.

Although quantifying deltaic island size is challenging and potentially subjective, we obtained estimates for the average and range of island sizes for the deltas in Figure 5d on the basis of 10–20 measurements from satellite images of the active delta topsets (Figures S12–S18 in Supporting Information S1); the Nile, Upper Rhone, Magdalena, and Yellow do not form islands. Under the base set of parameters, island sizes tended to be small compared to measurements (Figure 5d). However, we found that a modest increase in entrainment threshold can significantly increase predicted island size, which is reasonable if cohesive sediment or vegetation is present (Jacobs et al., 2011; Mitchener & Torfs, 1996). The island water level slope is also a major control; our assumption that the island slope is twice the delta slope decreased predicted island sizes, but without this assumption, we did not obtain a minimum stable island size for the Mississippi scenario. For most deltas, a combination of reduced island slope and increased entrainment threshold increased island sizes to within the measured ranges. We also found that a factor of two increase in RSLR has a negligible effect on minimum island size for bisection, but decreases the maximum stable island size. This suggests that the island size distribution of deltas will narrow under increased 21st century rates of RSLR due to bisection of large islands.

6. Discussion and Conclusions

Predictions of deltaic land loss are based primarily on calculating the sediment available to aggrade the delta top, assuming present-day delta shape, at the rate of RSLR (Giosan et al., 2014; Syvitski et al., 2009). These analyses have led to important and sometimes dire warnings about the fate of our coastlines (Blum & Roberts, 2009; Tessler et al., 2015). Our results do not contradict these warnings, but suggest that delta response to RSLR can be more dynamic.

Secondary channels with autogenic oscillations provide a mechanism for producing stable islands with a uniform aggradation rate keeping pace with RSLR on average, in contrast to the zero-entrainment model's non-uniform accretion rates. This suggests that islands do not passively drown if under-supplied with sediment. Instead, they self organize to deliver more sediment to the island interior, predominantly by maintaining larger and more persistent secondary channels. However, when the hydraulic slope is small, secondary channels are not always adequate for delivering sediment deep into the island interior, resulting in a quasi-stable condition where only part of the island keeps pace with RSLR. Furthermore, mass balance for the delta as a whole still applies: if islands upstream in the delta receive more sediment due to increased RSLR, then primary channel sediment concentrations decline farther downstream, causing islands to be unable to keep pace with RSLR. Here, secondary channels may act to increase sediment retention by routing sediment to islands where it can be more easily retained, rather than bypassing the delta through primary channels. Additionally, as discharge to islands increases, our assumption that the primary channel is unaffected by sediment and water loss to the island may break down, and as shown in Figure S11 of Supporting Information S1, island size predictions are sensitive to changes in primary channel concentration and depth.

Despite the simplified approach we use in this paper, our model generates complex and unexpected behavior, providing insight into a new potential mechanism for island accretion. Because our model is 1D, it does not include potentially important effects such as flow spreading or competition for nourishment area between multiple secondary channels within an individual island (Lazarus et al., 2020; Shaw et al., 2016), and does not yield a prediction for secondary channel width. We neglected sediment redistribution associated with tides and waves, which could compensate for the sediment deficit of the zero-entrainment model. We assumed constant river discharge, and although stage fluctuations are fast compared to decadal-scale island morphodynamics, they could enhance secondary channel erosion via higher water slopes during the hydrograph rising limb. Despite its simplicity, under certain realistic parameter choices, our model generates island sizes consistent with field estimates (Figure 5).

Whereas previous work has focused on the dynamics of channel-splitting to explain delta planform geometry (Edmonds & Slingerland, 2007; Ke et al., 2019; Shaw et al., 2018), our work indicates that deltaic island size is regulated by morphodynamic feedbacks. We found that large deltaic islands are inevitably bisected, implying that they are unstable features, which may help explain the observation across deltas of near-constant down-delta nearest-edge distances (Edmonds et al., 2011). In contrast, when small islands are separated by an unstable

bisecting channel, our model implies that the channel will aggrade, providing a potential mechanism for small islands to merge and form larger islands, as observed in Wax Lake Delta (Figures 1e and 1d). Based on these mechanisms, we hypothesize that islands in the active portion of river deltas self-organize to a size range spanning the minimum size for bisection and the maximum size for stability. Therefore, in addition to developing more persistent secondary channels that better nourish island interiors, our results suggest that natural deltas might also respond to RSLR by bisecting islands, resulting in smaller islands with more connectivity to the channel network, and therefore greater accretion rates (Edmonds et al., 2011; Passalacqua et al., 2013; Piliouras & Rowland, 2020). Overall, our model suggests that as long as sediment supply in the surrounding primary channels remains sufficient, islands self-organize in such a way to keep pace with increased RSLR.

Data Availability Statement

Model code and results can be downloaded from https://doi.org/10.3334/ORNLDAAC/2106.

Acknowledgments
The NASA Delta-X project is funded by the Science Mission Directorate's Earth Science Division through the Earth Venture Suborbital-3 Program NNH17ZDA001N-EVS3. The authors thank Marc Simard, Paola Passalacqua, Sergio Fagherazzi, and Justin Nghiem for insightful discussions.

References

Baptist, M., Babovic, V., Rodríguez Uthurburu, J., Keijzer, M., Uittenbogaard, R., Mynett, A., & Verwey, A. (2007). On inducing equations for vegetation resistance. *Journal of Hydraulic Research*, *45*(4), 435–450. https://doi.org/10.1080/00221686.2007.9521778

Blum, M. D., & Roberts, H. H. (2009). Drowning of the Mississippi Delta due to insufficient sediment supply and global sea-level rise. *Nature Geoscience*, *2*(7), 488–491. https://doi.org/10.1038/ngeo553

Brownlie, W. R. (1981). Prediction of flow depth and sediment discharge in open channels.

Chadwick, A. J., Lamb, M. P., & Ganti, V. (2020). Accelerated river avulsion frequency on lowland deltas due to sea-level rise. *Proceedings of the National Academy of Sciences of the United States of America*, *117*(30), 17584–17590. https://doi.org/10.1073/pnas.1912351117

Chow, V.T. (1959). *Open-channel Hydraulics*, McGraw-Hill. P. 680.

Day, G., Dietrich, W. E., Rowland, J. C., & Marshall, A. (2008). The depositional web on the floodplain of the Fly River, Papua New Guinea. *Journal of Geophysical Research*, *113*(1), 1–19. https://doi.org/10.1029/2006JF000622

Edmonds, D. A., Caldwell, R. L., Brondizio, E. S., & Siani, S. M. (2020). Coastal flooding will disproportionately impact people on river deltas. *Nature Communications*, *11*(1), 1–8. https://doi.org/10.1038/s41467-020-18531-4

Edmonds, D. A., Paola, C., Hoyal, D. C., & Sheets, B. A. (2011). Quantitative metrics that describe river deltas and their channel networks. *Journal of Geophysical Research*, *116*(4), F04022. https://doi.org/10.1029/2010JF001955

Edmonds, D. A., & Slingerland, R. L. (2007). Mechanics of river mouth bar formation: Implications for the morphodynamics of delta distributary networks. *Journal of Geophysical Research*, *112*(F2), F02034. https://doi.org/10.1029/2006JF000574

Esposito, C. R., Georgiou, I. Y., & Straub, K. M. (2020). Flow loss in deltaic distributaries: Impacts on channel hydraulics, morphology, and stability. *Water Resources Research*, *56*(5), 1–18. https://doi.org/10.1029/2019WR026463

Ganti, V., Lamb, M. P., & McElroy, B. (2014). Quantitative bounds on morphodynamics and implications for reading the sedimentary record. *Nature Communications*, *5*(1), 1–7. https://doi.org/10.1038/ncomms4298

Giosan, L., Syvitski, J., Constantinescu, S., & Day, J. (2014). Climate change: Protect the world's deltas. *Nature*, *516*(729), 31–33. https://doi.org/10.1038/516031a

Hiatt, M., & Passalacqua, P. (2015). Hydrological connectivity in river deltas: The first-order importance of channel-island exchange. *Water Resources Research*, *51*(4), 2264–2282. https://doi.org/10.1002/2014WR016149

Hiatt, M., & Passalacqua, P. (2017). What controls the transition from confined to unconfined flow? Analysis of hydraulics in a coastal river delta. *Journal of Hydraulic Engineering*, *143*(6), 03117003. https://doi.org/10.1061/(asce)hy.1943-7900.0001309

Hoitink, A. J., Nittrouer, J. A., Passalacqua, P., Shaw, J. B., Langendoen, E. J., Huismans, Y., & van Maren, D. S. (2020). Resilience of river deltas in the Anthropocene. *Journal of Geophysical Research: Earth Surface*, *125*(3), 1–24. https://doi.org/10.1029/2019JF005201

Jacobs, W., Le Hir, P., Van Kesteren, W., & Cann, P. (2011). Erosion threshold of sand-mud mixtures. *Continental Shelf Research*, *31*(10), S14–S25. https://doi.org/10.1016/j.csr.2010.05.012

Ke, W.-T., Shaw, J. B., Mahon, R. C., & Cathcart, C. A. (2019). Distributary channel networks as moving boundaries: Causes and morphodynamic effects. *Journal of Geophysical Research: Earth Surface*, *124*(7), 1878–1898. https://doi.org/10.1029/2019JF005084

Kirwan, M. L., Guntenspergen, G. R., D'Alpaos, A., Morris, J. T., Mudd, S. M., & Temmerman, S. (2010). Limits on the adaptability of coastal marshes to rising sea level. *Geophysical Research Letters*, *37*(23), L23401. https://doi.org/10.1029/2010GL045489

Lazarus, E. D., Davenport, K. L., & Matias, A. (2020). Dynamic allometry in coastal overwash morphology. *Earth Surface Dynamics*, *8*(1), 37–50. https://doi.org/10.5194/esurf-8-37-2020

Lorenzo-Trueba, J., Voller, V. R., Paola, C., Twilley, R. R., & Bevington, A. E. (2012). Exploring the role of organic matter accumulation on delta evolution. *Journal of Geophysical Research*, *117*(F4), F00A02. https://doi.org/10.1029/2012JF002339

Mitchener, H., & Torfs, H. (1996). Erosion of mud/sand mixtures. *Coastal Engineering*, *29*(1–2), 1–25. https://doi.org/10.1016/S0378-3839(96)00002-6

Nienhuis, J. H., Ashton, A. D., Edmonds, D. A., Hoitink, A. J., Kettner, A. J., Rowland, J. C., & Törnqvist, T. E. (2020). Global-scale human impact on delta morphology has led to net land area gain. *Nature*, *577*(7791), 514–518. https://doi.org/10.1038/s41586-019-1905-9

Nienhuis, J. H., Törnqvist, T. E., & Esposito, C. R. (2018). Crevasse splays versus avulsions: A recipe for land building with levee breaches. *Geophysical Research Letters*, *45*(9), 4058–4067. https://doi.org/10.1029/2018GL077933

Paola, C., Twilley, R. R., Edmonds, D. A., Kim, W., Mohrig, D., Parker, G., et al. (2011). Natural processes in delta restoration: Application to the Mississippi Delta. *Annual Review of Marine Science*, *3*(1), 67–91. https://doi.org/10.1146/annurev-marine-120709-142856

Parker, G. (2004). 1D sediment transport morphodynamics with applications to rivers and turbidity currents. E-book available at Gary Parker's Morphodynamics Web Page, last update April 2006.

Parker, G., Garcia, M., Fukushima, Y., & Yu, W. (1987). Experiments on turbidity currents over an erodible bed. *Journal of Hydraulic Research*, *25*(1), 123–147. https://doi.org/10.1080/00221688709499292

Passalacqua, P., Lanzoni, S., Paola, C., & Rinaldo, A. (2013). Geomorphic signatures of deltaic processes and vegetation: The Ganges-Brahmaputra-Jamuna case study. *Journal of Geophysical Research: Earth Surface*, *118*(3), 1838–1849. https://doi.org/10.1002/jgrf.20128

Piliouras, A., & Rowland, J. C. (2020). Arctic river delta morphologic variability and implications for riverine fluxes to the coast. *Journal of Geophysical Research: Earth Surface*, *125*(1), 1–20. https://doi.org/10.1029/2019JF005250

Rouse, H. (1937). Modern conceptions of the mechanics of fluid turbulence. *Transactions of the American Society of Civil Engineers*, *102*(1), 463–505. https://doi.org/10.1061/taceat.0004872

Rowland, J. C., Dietrich, W. E., Day, G., & Parker, G. (2009). Formation and maintenance of single-thread tie channels entering floodplain lakes: Observations from three diverse river systems. *Journal of Geophysical Research*, *114*(2), F02013. https://doi.org/10.1029/2008JF001073

Shaw, J. B., Miller, K., & McElroy, B. (2018). Island formation resulting from radially symmetric flow expansion. *Journal of Geophysical Research: Earth Surface*, *123*(2), 363–383. https://doi.org/10.1002/2017JF004464

Shaw, J. B., Mohrig, D., & Wagner, R. W. (2016). Flow patterns and morphology of a prograding river delta. *Journal of Geophysical Research: Earth Surface*, *121*(2), 372–391. https://doi.org/10.1002/2015JF003570

Shields, M. R., Bianchi, T. S., Mohrig, D., Hutchings, J. A., Kenney, W. F., Kolker, A. S., & Curtis, J. H. (2017). Carbon storage in the Mississippi River delta enhanced by environmental engineering. *Nature Geoscience*, *10*(11), 846–851. https://doi.org/10.1038/NGEO3044

Slingerland, R., & Smith, N. D. (1998). Necessary conditions for a meandering-river avulsion. *Geology*, *26*(5), 435–438. https://doi.org/10.1130/0091-7613(1998)026<0435:NCFAMR>2.3.CO;2

Sturm, T. (2010). *Open channel hydraulics*. McGraw-Hill. Retrieved from https://books.google.com/books?id=cOUiPwAACAAJ

Syvitski, J. P., Kettner, A. J., Overeem, I., Hutton, E. W., Hannon, M. T., Brakenridge, G. R., et al. (2009). Sinking deltas due to human activities. *Nature Geoscience*, *2*(10), 681–686. https://doi.org/10.1038/ngeo629

Tessler, Z., Vörösmarty, C. J., Grossberg, M., Gladkova, I., Aizenman, H., Syvitski, J. P., & Foufoula-Georgiou, E. (2015). Profiling risk and sustainability in coastal deltas of the world. *Science*, *349*(6248), 638–643. https://doi.org/10.1126/science.aab3574

Trampush, S. M., Huzurbazar, S., & McElroy, B. (2014). Empirical assessment of theory for bankfull characteristics of alluvial channels. *Water Resources Research*, *50*(12), 9211–9220. https://doi.org/10.1002/2014WR015597

Vanoni, V. A. (1946). Transportation of suspended sediment by water. *Transactions of the American Society of Civil Engineers*, *111*(1), 67–102. https://doi.org/10.1061/taceat.0005975

van Rijn, L. C. (1984). Sediment transport, part ii: Suspended load transport. *Journal of Hydraulic Engineering*, *110*(11), 1613–1641. https://doi.org/10.1061/(ASCE)0733-9429(1984)110:11(1613)

References From the Supporting Information

An, C., Moodie, A. J., Ma, H., Fu, X., Zhang, Y., Naito, K., & Parker, G. (2018). Morphodynamic model of the lower yellow river: Flux or entrainment form for sediment mass conservation? *Earth Surface Dynamics*, *6*(4), 989–1010. https://doi.org/10.5194/esurf-6-989-2018

de Leeuw, J., Lamb, M. P., Parker, G., Moodie, A. J., Haught, D., Venditti, J. G., & Nittrouer, J. A. (2020). Entrainment and suspension of sand and gravel. *Earth Surface Dynamics*, *8*(2), 485–504. https://doi.org/10.5194/esurf-8-485-2020

Ferguson, R., & Church, M. (2004). A simple universal equation for grain settling velocity. *Journal of Sedimentary Research*, *74*(6), 933–937. https://doi.org/10.1306/051204740933

Wright, S., & Parker, G. (2004). Flow resistance and suspended load in sand-bed rivers: Simplified stratification model. *Journal of Hydraulic Engineering*, *130*(8), 796–805. https://doi.org/10.1061/(ASCE)0733-9429(2004)130:8(796)